Development of JET Hybrid Scenario Plasmas in Deuterium and Deuterium-Tritium for Impurity Screening Investigations

D. B. King[1], A.Field[1], C.D. Challis[1], J.Hobirk[2], A. Kappatou[2], E.A. Lerche[3], D. Keeling[1], M. Baruzzo[4], I.S. Carvalho[5], P.Carvalho[1], E.G. Delabie[6], J.M. Fontdecaba [7], L. Frassinetti[8], ,C. Giroud[1], K. Kirov[1], E. Litherland-Smith[1], M. Maslov[1], A.Meigs[1], S.Menmuir[1], C.Olde[1], G. Pucella[9], S. Silburn[1], H.Sun[1] , JET contributors ‡ and the Eurofusion Tokamak Exploitation Team §

Eurofusion Consortium JET, Culham Campus, Abingdon, OX14 3DB, UK [1] UKAEA, Culham Campus, Abingdon, UK, [2] Max-Planck-Institut fr Plasmaphysik, Boltzmannstr. 2, 85748 Garching, [3] LPP-ERM/KMS, Brussels, Belgium, [4] Consorzio RFX, Padova, Italy, [4] ITER Organisation, Route de Vinon-sur-Verdon, CS 90 046, 13067 St Paul Lez Durance Cedex, France, [5] Queens University, Belfast, UK, [6] Oak Ridge National Laboratory, Oak Ridge, USA, [7] Laboratorio Nacional de Fusin. Ciemat, 28040 Madrid, Spain, [8]Fusion Plasma Physics, EECS, KTH Royal Institute of Technology, SE-10044 Stockholm, Sweden, [9]ENEA C. R. Frascati, 00044 Frascati (Roma), Italy

E-mail: damian.king@ukaea.uk

Abstract.

The low density and high temperature at the pedestal in hybrid scenarios on JET provide a unique test of the neo-classical screening in the periphery of the plasma that has previously been observed on JET in such plasmas. Hybrid scenario plasmas have been further developed to aid in the study of temperature gradient screening of high-Z impurities from the core of the plasma via plasma current, toroidal field, gas fuelling, density and isotope variations. The steps required to adapt the pulses from deuterium to deuterium-tritium are discussed and provide some guidance for future experiments that may operate in deuterium-tritium. The optimisation of the scenario allowed for improved bolometry data compared to the Deuterium Tritium Experiment 2 (DTE2) campaign on JET, hence this work provides vital evidence of impurity screening in a high fusion power, deuterium-tritium plasma.

‡ See the author list of C.F. Maggi et al 2024 Nucl. Fusion **64** *112012*
§ See the author list of E. Joffrin et al 2024 Nucl. Fusion **64** *112019*

1. Introduction

On fusion devices with tungsten plasma facing components the radiation losses can cause significant plasma cooling if the tungsten reaches the core of the plasma, this can indeed be the limiting factor in successful plasma discharges. There are a number of effects that may prevent or reduce the source or transport of this influx, one such effect is the screening of tungsten from the core due to neoclassical convection in the situation where the ion temperature gradient is sufficiently high compared to the electron density gradient. For ITER plasmas this "temperature gradient screening" is predicted [1] and is important for successful ITER plasma operations.

This impurity screening in the periphery of the plasma has been successfully demonstrated on the JET tokamak as part of the hybrid plasma scenario development [2]. The hybrid scenario on JET was developed in order to achieve high fusion power and was typically characterised by a broad q-profile with q_{min} slightly above 1 and $\beta_N > 2$ [3]. These plasmas provide good conditions for screening thanks to high input power, low collisionality and strong rotation. These effects were also seen during the Deuterium Tritium Experiment 2 (DTE2) experiments on JET [4] [5]. Further investigations into this effect were carried out and continued into the Deuterium Tritium Experiment 3 (DTE3) campaign [6] [7].

To access the screening conditions on JET the hybrid scenario pulses have been optimised to achieve low pedestal density ($n_{e,ped}$), and high ion pedestal temperature ($T_{i,ped}$), and consequently a low collisionality and strong rotation which lead to neoclassical screening as discussed in [8]. To achieve this on JET an optimised gas fuelling timing is used, with a phase of no gas injection at the beginning of the high power phase to build up a strong temperature pedestal, followed by a timed gas puff to trigger the first edge localised modes (ELMs). This is to avoid having a very large first ELM that brings in large amounts of tungsten degrading the pedestal temperature leading to reduced overall plasma fusion power and removing any possible screening. The input power is provided by Neutral Beam Injection (NBI) and Ion Cyclotron Resonant Heating (ICRH).

As part of the experiment variations, in plasma density were performed to attempt to quantify the impact on screening. This was achieved by varying plasma current, affecting particle confinement and/or gas fuelling. Further variations performed were in NBI configuration to adjust rotation and in plasma isotope by performing experiments in deuterium-tritium (DT) compared to pure deuterium (D). As part of the development of DT plasmas the toroidal field was also increased to account for changes to H-mode entry associated with isotope dependence, rather than to determine an explicit dependence of the screening effect on toroidal field.

The presence of impurity screening in JET plasmas is assessed by detailed examination of bolometry data as in [2]. The method discussed in this paper show how in some cases impurity screening can occur in the inter-ELM phase and how in other cases the impurities are flushed out by the ELM in a more standard way. This analysis shows strong screening in many of the pulses performed, including those in DTE3. Due to the dependence of the study on bolometry, further development to ensure good quality data was required. Analysis of the plasma profiles with FACIT [8] can determine if a given time point in a plasma is in the conditions required for neoclassical screening or not. This analysis and the outcome of this are the subject of a separate publication [9]. Here the scenario development and experimental observations are presented.

2. Scenario Development in Deuterium

The goal of the experiments was to develop hybrid plasmas that could explore the peripheral screening further to the work presented in [2] and to prepare for possible experiments in DT with improved diagnostic coverage compared to the previous results. The starting point was the best results from the previous data, in particular the pulse 97781 as analysed in [2]. Given the dependence of the results of neoclassical screening on density, ion temperature gradients and on rotation these were the parameters that were desirable to modify. However, on JET it is not straightforward to independently vary these parameters.

As the maximum available input power on JET was required to access screening conditions and a stable scenario [2][4], changing the input power is not a viable path to adjust the impurity screening. Pulses within the development of the scenario that had lower power would typically fail due to strong impurity accumulation related to a combination of too-low a temperature for impurity screening while also having too-low an ELM frequency for impurity flushing [4]. If the input power is fixed then a change in the density will also lead to a change in temperature and also to the resulting rotation in the plasma. Thankfully at least these coupled changes at least are expected to have a consistent effect on the screening, i.e. if the density decreases and then the temperature increases then both of these effects should lead to an increase in neoclassical screening.

Additionally, there were some issues with available diagnostics necessary to the study of impurity screening. These issues were: uncertainty in the

ion temperature profile, bolometer data being affected by main chamber gas puffing during DT experiments and the lack of diagnostics showing the source of impurities from the divertor. A further goal of the new experiments was to mitigate these issues by adapting the plasma scenario where possible.

2.1. Parameter variations in Plasma to Study Screening

The hybrid scenario on JET in preparation for DTE2 had primarily operated at 2.3MA/3.45T, this operating point was chosen following optimisation studies carried out in [4] to maximise fusion performance as defined by high neutron rates which requires high core plasma temperature and low core impurity radiation. The toroidal field was chosen based on the ICRH frequencies available while the plasma current was chosen based on the q95 desired for a hybrid plasma with further refinement based on considerations such as the optimal density for fusion performance on JET and the avoidance of hotspots on the main chamber caused by ICRH accelerated fast particles. Integrated modelling [10] had been performed to support this optimisation and assist in the scoping of the experiments, this was also used to follow a predict-first approach to expected fusion power. Plasma currents of 2.1-2.5MA had been attempted in this scenario before [4], with the higher currents providing lower performance due to higher densities and the lower currents having transiently improved performance but issues with the hotspots. Following these tests the further development of the scenario was focussed on 2.3MA plasmas.

A plasma similar to 97781 at 2.3MA/3.45T was established to achieve this, some variation in the gas levels of the original pulse were required, the gas setup is shown in Fig. 1. This gas waveform is optimised to allow for the highest plasma temperature in the H-mode entry phase, during which the plasma performance peaks before reducing to a stationary state, while ensuring the first ELM is not so large as to degrade performance. The main phase gas is also optimised so that the ELM frequency is not so high that the analysis of the inter-ELM phase is impossible while also ensuring that the ELM frequency is not so low as to cause impurity influx due to ELMs that are too large.

Following this the first variation attempted as part of the study was a reduction in plasma current to lower the plasma density. A number of plasmas were successfully run at 2.1MA (pulse 102825) and provided a variation compared to 2.3MA (pulse 102813). The variation in plasma current provided the desired change in plasma density and temperature as shown in Fig. 2, the rotation has also changed slightly as can be seen in Fig.3. The ion temperature shown here is a fixed position that is close to the plasma edge but inside of the pedestal. There is a difference in the input power between the two pulses although this is considered small, also in the first $\sim 2s$ of the pulse the lower NBI power is compensated by the higher ICRH power. There is also a difference in the gas waveform, this was found to be necessary to account for a small variation in first ELM timing when the plasma current was changed.

The raw data and fitted profiles of these pulses are shown in Fig.3 where it can be seen that the density pedestal in the 2.1MA plasma is lower than the 2.3MA case. Ion temperature data is measured by charge-exchange-recombination spectroscopy (CXRS) systems. The data is obtained from a core system [11] (labelled CXG6 in Fig. 3) and an edge system [12] (labelled CX7C and CX7D in Fig. 3) then combined and fitted, details of the fitting and issues with the data are discussed in [9].

There was a concern based on previous experiments [13] that there may be overheating of some limiters due to unconfined fast particles related to NBI-ICRH synergies. While there was heating of the limiters this was not at a level that caused a problem for the pulse, this was likely due to appropriate gas dosing near the ICRH antenna which has proved to be successful at mitigating this issue in the past [13][4]. An example of the heating of one of these components is shown in Fig.4 where the limit for the temperature of this limiter is 950^oC.

It was desirable to adjust the rotation of the plasma without a change in density to isolate that aspect of the impurity screening behaviour. An attempt was made with an adjustment to the NBI configuration. The NBI on JET is split on each beamline into two banks [14], one of which is more tangential than the other. These banks are referred to as "NORM" for the more normal angle injection and "TAN" for the more tangential. In principle different combinations of NBI power can provide different amounts of torque and hence rotation, however as all input power is required for these hybrid plasmas there is a limit to how large a variation can be achieved. Further to this, there are different NBI shinethrough requirements for the different banks and it is not straightforward in an optimised scenario to adjust them. The pulses had been optimised with the first bank operating at slightly lower energy while the density is lower to avoid excessive shinethrough while the second bank operating at higher energy when the density has started to rise. The NBI order and energies are shown in Fig. 5

With a change to the NBI energies used, such that the NBI bank on first is at the lowest energy and

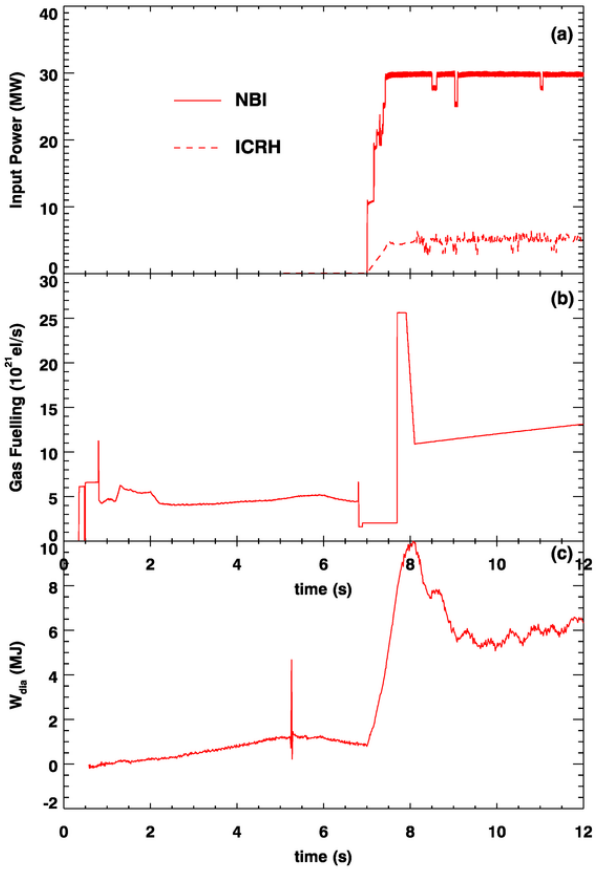

Figure 1: *Input power, NBI solid and ICRH dashed (a) gas waveforms (b) and resulting stored energy of example hybrid plasma.*

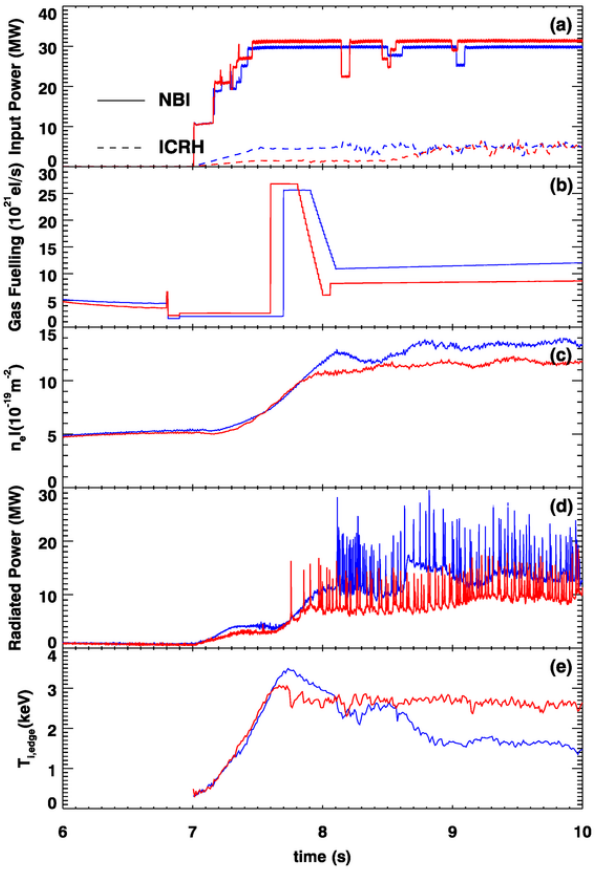

Figure 2: *Comparison of 2.1MA (red, 102825) and 2.3MA (blue, 102813) plasmas. Input power , NBI solid and ICRH dashed (a), gas fuelling (b), line integrated density (c), Radiated power (d) and edge ion temperature (e).*

hence has the most relaxed shinethrough requirements, it was possible to perform two pulses with the TAN and NORM banks in a different order in the power ramp in an attempt to change the initial torque, although the main phase torque would remain the same. Unfortunately in the conditions of these plasmas this made no measurable change to the rotation in the edge of the plasma

The final part of the experiment in deuterium plasmas was the variation of the density at constant plasma current by changes to the gas fuelling. This was performed in two separate ways, firstly by lowering the plasma density at the start of the NBI and secondly by the delay in the gas puff to trigger the first ELM. The variation in gas puff and resulting changes to the plasma density, edge ion temperature and impurity radiation are shown in Fig. 6 while the variation in pre-heat density is shown in Fig. 7. These scans were successful, partly due to consistent plasma conditions and input power over the scans.

In the variation of the gas puff timing it was observed that with very early or very late gas puff the plasma performance was reduced. An early gas puff prevented the development of a high ion temperature and had increased impurity radiation, while a late gas puff led to a very large first ELM and reduced performance. This reflected the earlier work on optimisation of the hybrid plasma gas fuelling, discussed in detail in [4], but here performed in more controlled conditions over a wider range of gas puff timing.

The changes to pre-heat density had a similar effect, with too high a density leading to poor performance and higher impurity radiation. The data for the denstiy variation is shown in the same way as for the gas puff timing in Fig. 7

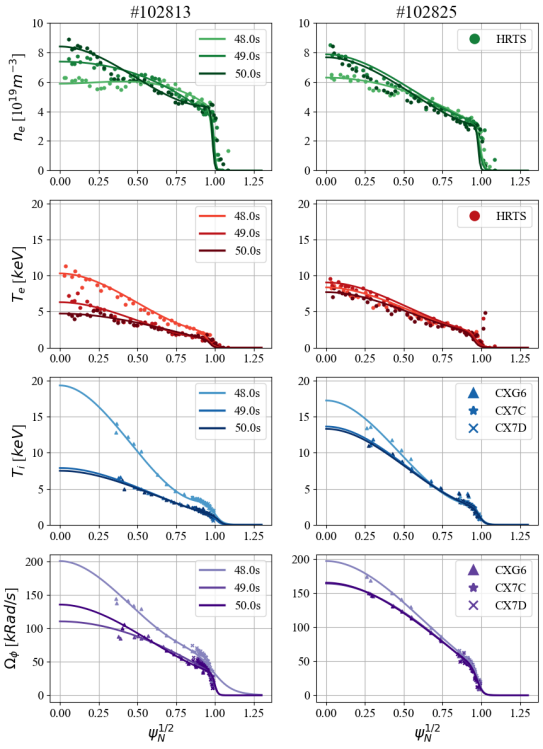

Figure 3: *Density (top), electron temperature (second), ion temperature (third) and rotation (bottom) for the 2.1MA and 2.3MA plasmas at different times in the evolution of the pulse.*

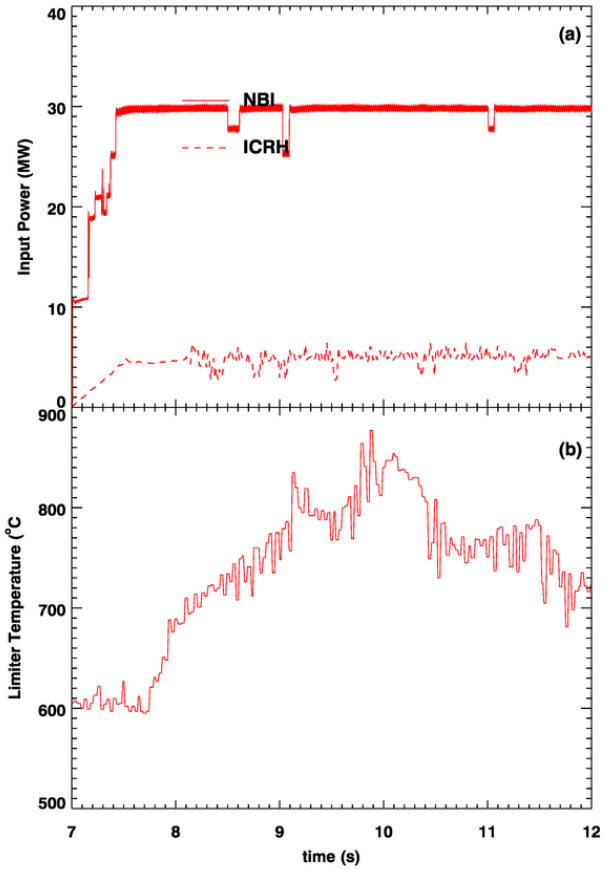

Figure 4: *Heating of the wide outer poloidal limiter, temperature limit of this component is 950°C*

3. Preparation for Deuterium-Tritium

The injection of tritium into JET plasmas is done via the Tritium Introduction Modules (TIMs) [15]. These TIMs have different gas flow characteristics to the standard Gas Injection Modules (GIMs) due to the longer pipework required and are also in fewer locations around the vessel, the locations are shown in Fig. 8. There are 3 TIMs in the divertor and 2 in the main chamber. Those in the divertor are slower to start delivering gas and reach the maximum gas flow rate in the torus than those in the main chamber. As the gas fuelling optimisation for these plasmas requires a fast response from the gas injection the use of the TIMs causes issues. This is further complicated by the impact the faster, main chamber TIMs have on the bolometry data due to the proximity to the bolometer cameras [4]. As the bolometry data is essential for the analysis, those TIMs should be avoided as much as possible. In contradiction to this requirement, the ICRH coupling with the plasma is improved by the use of main chamber gas, whether D or T.

The previous hybrid development in DTE2 had used one of the faster, main chamber TIMs (TIM 15) to inject tritium and the standard main chamber GIMs to inject deuterium, this TIM was chosen to be as similar to the fuelling behaviour of the previously used GIMs as possible. The NBI system was also used in a mixture of D and T providing approximately balanced fuelling. Due to this use of TIM15, the quality of DTE2 bolometry data was reduced. In DTE2 plasmas TIM15 fulfilled two roles, (1) to provide balanced DT, plasma density control in the pre-heat phase and (2) to provide T dosing during the main H-mode phase.

The strategy devised for DTE3 was to retain the use of TIM15 for the density control during the pre-heat phase as the bolometry was of less interest here and then to use a different TIM during the main phase. The fast injection of gas to trigger the first ELM would all be deuterium provided by 2 main chamber GIMs (numbered 1 and 6) as in the deuterium plasmas already described, because the divertor TIMs could not respond quickly enough. A further change for DTE3

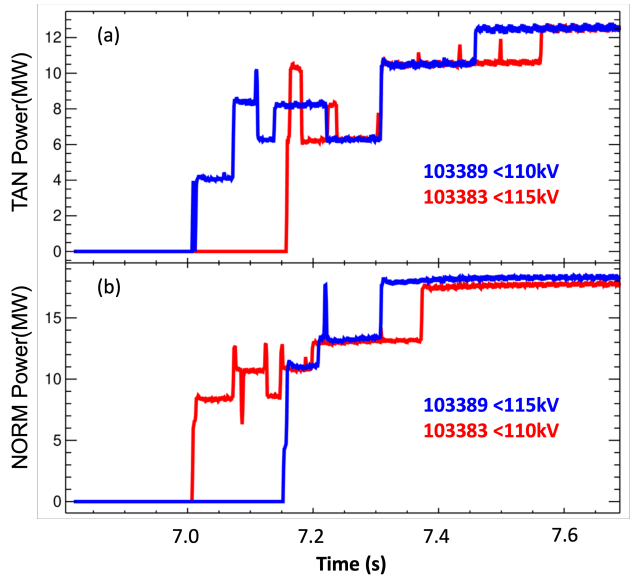

Figure 5: *Variation in the order of TAN and NORM NBI power. In (a) the TAN power is shown for two pulses with different maximum NBI energy, in (b) the NORM power for the same pulses is shown.*

compared to DTE2 was that all of the NBI was in D in DTE3 while in DTE2 it was a roughly equal mixture of D and T. As this large injection of D combined with the all D fuelling from the NBI would change the isotope ratio it was decided to begin the pulse with all T gas fuelling to attempt to compensate for this. While this variation in DT ratio is not desirable it was considered a worthwhile compromise to obtain good quality data. A schematic of this approach is shown in Fig. 9. The "gap" in fuelling was as previously shown to allow a high temperature pedestal but also to account for the slower turn-off characteristic of the TIM, particularly when using T2 rather than D2 which has a slower response due to pipework and also due to the isotope with a scaling of $\sqrt{M3/M2}$.

To test this change to the gas strategy before going to DT operations plasmas in D with a similar combination of injection points were attempted. Firstly, the gas dosing in the main phase was moved to the divertor (GIM10) and later to the equivalent TIM (TIM10) still fed with deuterium gas. On moving the gas to GIM10 the level was decreased by $\sim$ 10% to give an ELM frequency comparable to the existing main chamber gas pulses. This was required due to the variation in fuelling efficiency between divertor and main chamber. A comparison of a pulse with main chamber gas and divertor gas is shown in Fig.10. It can be seen that a similar performance has been achieved in the main phase with controlled radiation and an ELM frequency of $\sim$40Hz. It should be noted that the gas fuelling plot does not consider the difference in the

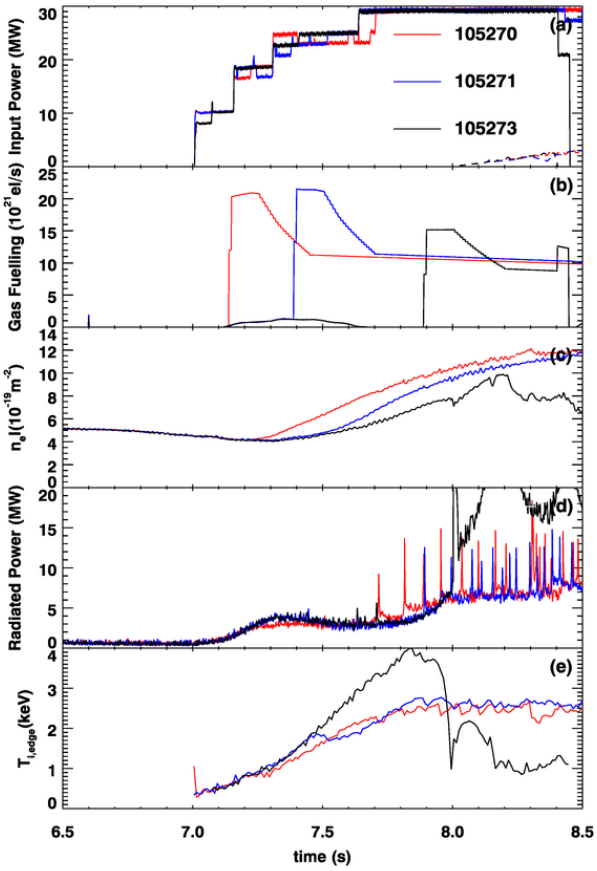

Figure 6: *Plasma behaviour with varying gas puff timing. Shown in (a) is the heating power, NBI solid and ICRH dashed, (b) is the gas fuelling rate, (c) is the line integrated plasma density, (d) is the total radiation power and (e) is the edge ion temperature*

response time and fuelling efficiency of the different locations, the large initial level in the divertor fuelled pulse is used to increase the response time of that GIM and does not mean that a much larger actual gas flow was present at that time. There is a difference in the beginning of the heating phase related to the delay between the valves and it was necessary to resolve that in the DT plasmas.

To adjust for the response rate of the GIMs versus TIMs a series of test pulses without plasma (known as dry runs) were performed which included injection from TIM15, TIM10 and GIM10. The data from the Penning gauges on the ICRH antenna provide a good main chamber measurement of the pressure that can be used to confirm the gas is arriving into the torus at the same time, as shown in Fig. 11. There are multiple gauges within different ICRH antennas around JET, these systems are divided into A, B, C and D and then further divided by number as shown in [16] . From

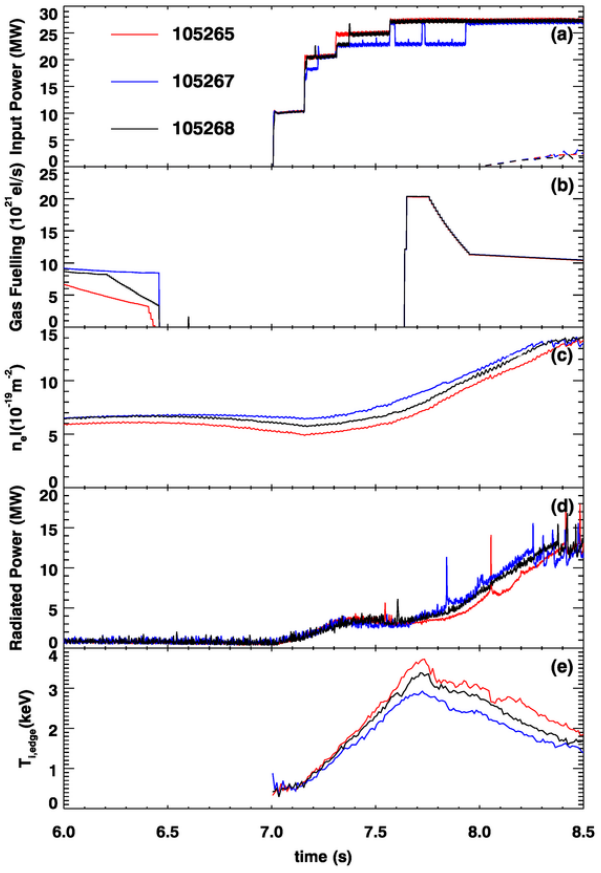

Figure 7: *Plasma behaviour with varying pre-heat plasma density. Shown in (a) is the heating power, NBI solid and ICRH dashed, (b) is the gas fuelling rate (note that gas puff after heating is constant between pulses so these overlap), (c) is the line integrated plasma density, (d) is the total radiated power and (e) is the edge ion temperature*

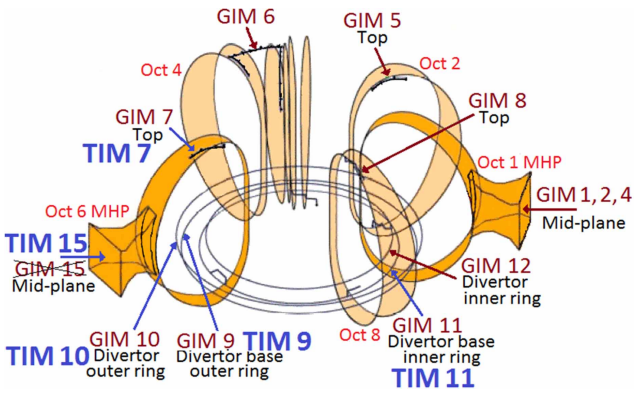

Figure 8: *Location of gas fuelling modules (GIMs and TIMs) on JET. Injection lines (shown in black) have simple holes through which the gas in injected. Reproduced from [15]*

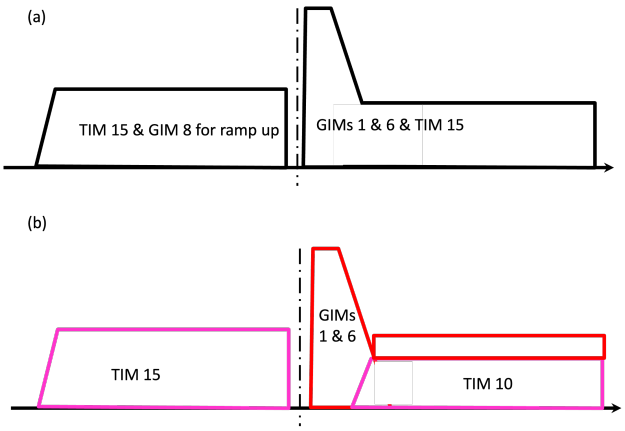

Figure 9: *Strategy for gas usage in the DT plasmas, (a) shows the strategy used in DTE2 with all gas shown together, (b) shows the strategy used in DTE3 with tritium injection shown in magenta and deuterium injection shown in red, the dashed line represents the heating start time in both plots.*

this data it could be seen that the delay between TIM 10 and TIM 15 with this programmed waveform was negligible across the three difference gauges.

The use of a pure tritium plasma during the ramp of the pulse required a further adaptation to the pulse setup. The density during the gas ramp is tuned to avoid hollow temperature profiles [17] leading to early disruptions. The density in this phase also affects the q-profile that has been highly tuned for hybrid plasmas. As part of the DTE2 hybrid development a variation in this density in both DT and pure T was performed, therefore the optimum density for a pure T (or close to it) plasma was available as a starting point [4].

4. Optimisation in DT

The first part of the DT experiments involved ohmic plasma tests to ensure that the ramp designed above for optimal q-profile was achieved. There are two criteria used in this part of the development, the avoidance of hollow temperature profiles and the arrival time of the first sawtooth when no heating is applied [17]. By comparing the ohmic pulse in DT with those in D it was possible to demonstrate whether this had been achieved. The use of an ohmic pulse is necessary to observe the first sawtooth with minimal use of tritium or production of 14MeV neutrons, both of which are subject to strict operational budgets [7]. A comparison of the ohmic plasmas is shown in Fig. 12, from which it can be seen that the end result was successful with the $q = 1$ arrival time in the DT ohmic pulse matching that of the D ohmic pulse.

In DT conditions it was expected that some minor tuning to the gas rates would be required but that

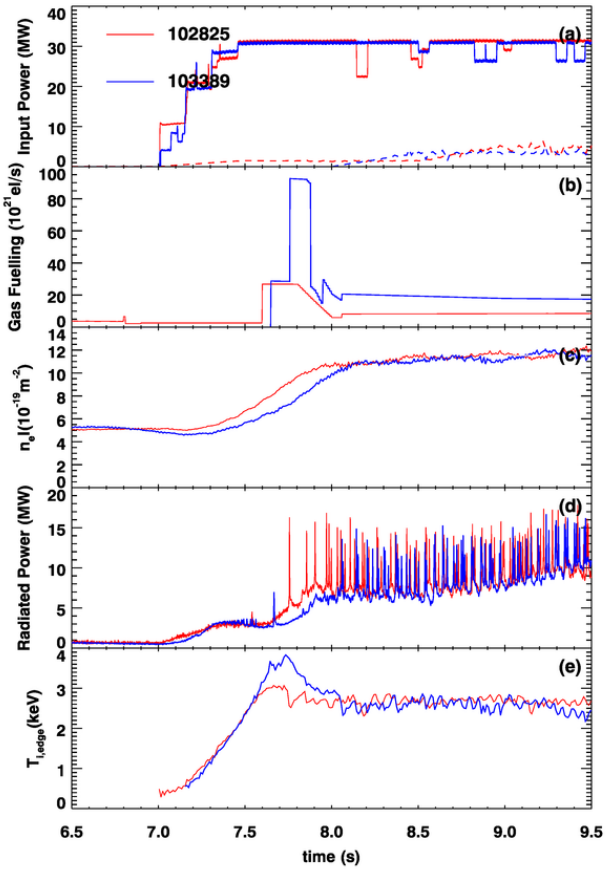

Figure 10: *Comparison of main chamber gas fuelling (red) and divertor, tritium compatible fuelling (blue). Shown in (a) is the heating power, NBI solid and ICRH dashed, (b) is the gas fuelling rate, (c) is the line integrated plasma density, (d) is the total radiated power and (e) is the edge ion temperature Both pulses used deuterium only.*

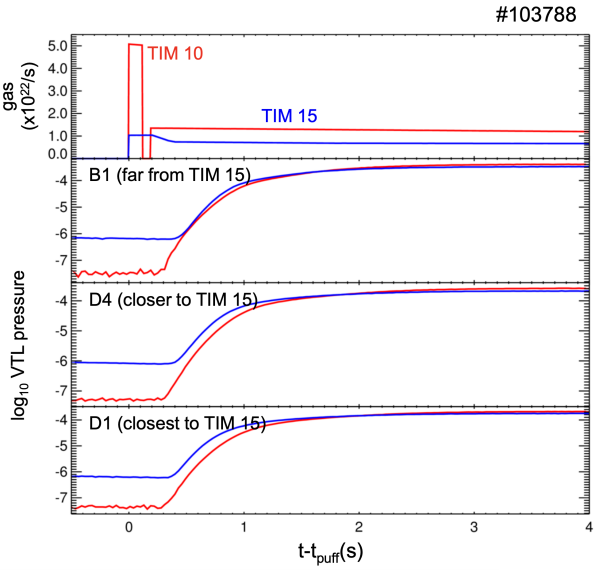

Figure 11: *Pressure measurements within different ICRH transmission lines B1, D4 and D1 [16] in response to gas puffs to confirm arrival time of gas into the vessel in dry runs. The gas puffs are separated in time within the same pulse and time shifted in these plots to align the starting time.*

the preparations in D would minimise these. The first pulse exhibited similar initial ion temperature in the pedestal compared to the reference pulses however the density in the ramp of the input power rose slightly more quickly than in D. This is due to the lower power required to enter H-mode in tritium plasmas [18], so the point in the ramp that the plasma entered H-mode and had higher density was moved earlier. This pulse had a larger amount of radiated power leading to a radiative collapse. This is consistent with the increased density in DT [19][20] reducing the screening of impurities although a detailed analysis of this failure has not yet been carried out and other causes for the failure of the pulse are possible.

To compensate for this effect the power in the ramp was adjusted such that H-mode entry was matched more closely to that of the plasmas in

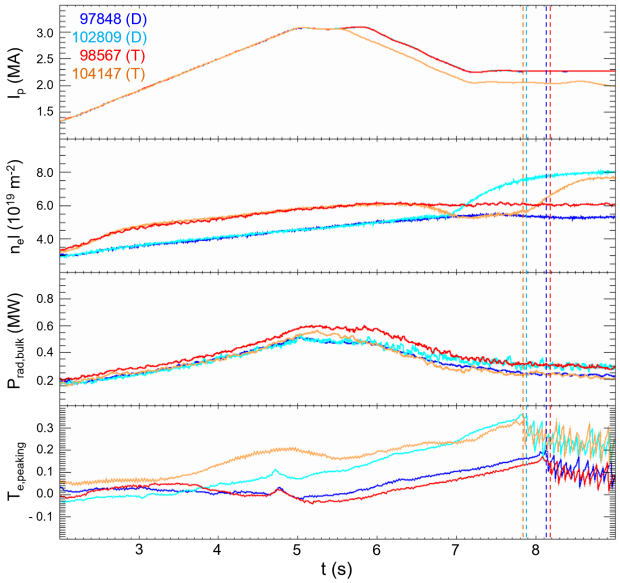

Figure 12: *Comparison of ohmic plasmas to assess $q = 1$ arrival time. Plasma current, line integrated density, radiated power and temperature peaking are shown. Can see that cyan and orange 2.1MA pulses have first sawtooth at the same time, earlier pulses at 2.3MA with matching sawtooth arrival shown in red and blue for comparison*

deuterium. The H-mode entry can be seen in Fig. 13. The black curve (DT) in panel (a) has slightly lower power during the NBI power ramp phase than the blue curve (DT) and hence the H-mode entry trajectory is altered. The density ramp rate was reduced very slightly (due to the change in H-mode entry timing) although still not to the level of the deuterium pulse, however this also went against the goal of maximising the temperature in the plasma. Some further tuning of the timing of the gas to trigger the first ELM [4] at the desired time was carried out and this provided some minor improvement in the performance. The gas injected in the main phase of the pulse from TIM10 was appropriate to stimulate ELMs that were not too frequent to prevent analysis of the data during inter-ELM periods. A comparison of the pulse in D (103793), the full ramp in DT (104215) and the adjusted ramp in DT (104216) is shown in Fig. 13. Note that the full power ramp pulse 104215 is terminated and power ramped down due to the high radiated power. The isotope ratio as measured in the sub-divertor is shown also to demonstrate how this ratio is varying during the pulse.

A number of the pulses demonstrated strong MHD activity, in particular 3/2 modes, which reduce the plasma performance. While this was undesirable it was not a barrier to the analysis of the screening behaviour in this case, particularly during the initial phase as there was typically a smaller effect on the plasma periphery and there was long enough before the mode to complete the analysis. Hence no action was taken to compensate for the modes given the short experimental time available. There was some variation in the onset of this mode even with minor changes in plasma conditions, however those pulses with stronger ramps in β_N exhibited an earlier onset time of this mode as shown in Fig. 16

To avoid the early H-mode entry related to the isotope and thereby be able to maintain full power in the ramp it was decided to increase the toroidal field as the LH threshold power typically increases with toroidal field [18][21] . Hybrid like plasmas in tritium rich conditions had already been performed in DTE2 at 3.85T as part of the fusion power optimised scenario [22]. As part of the development of that scenario a comparison of the $q = 1$ arrival time was performed, these showed that there was no change to the arrival time, this is likely due to the faster ramp of the toroidal field used for the 3.85T plasma

Three pulses were performed at 2.1MA/3.85T with some variation in the gas fuelling used. The first attempt, 104406, showed the entry to H-mode at the desired time with high pedestal temperature and controlled impurity radiation. However, the gas level in the main phase was now too high and the

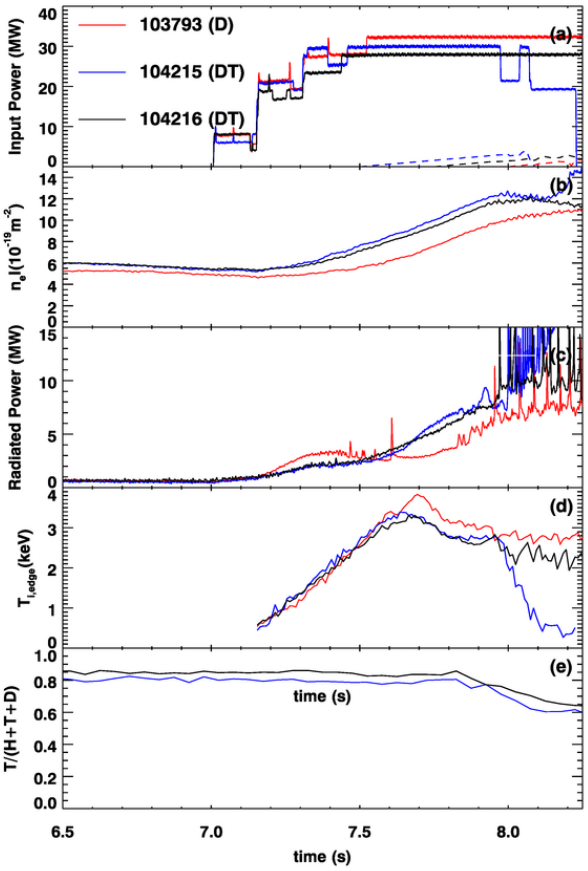

Figure 13: *H-mode entry in D (red, 103793) and DT with faster power ramp (blue, 104215) and DT with slower power ramp (black, 104216). Input power, NBI solid and ICRH dashed (a), line integrated density (b), radiated power (c), edge ion temperature (d) and tritium concentration (e)*

ELM frequency too high to be able to perform the inter-ELM analysis. For the following pulse, 104407, the gas level was reduced but the input power was insufficient. Finally, on pulse 104408 the gas level was reduced further and the input power of 33MW was achieved. However, on this pulse the gas level had been reduced too much and the pulse suffered from impurity accumulation in the main phase. These three pulses are compared in Fig. 14. Despite the issues encountered during the main phase these pulses provided good data during the initial overshoot phase and demonstrated strong ITBs, while the 3/2 mode was also still present.

Analysis of the bolometry data from the pulses with the use of divertor T fuelling was carried out in parallel with ongoing experiments. It was shown that even with this pulse setup the bolometer still suffered from some interference from this TIM gas. To further reduce this interference it was decided to remove the

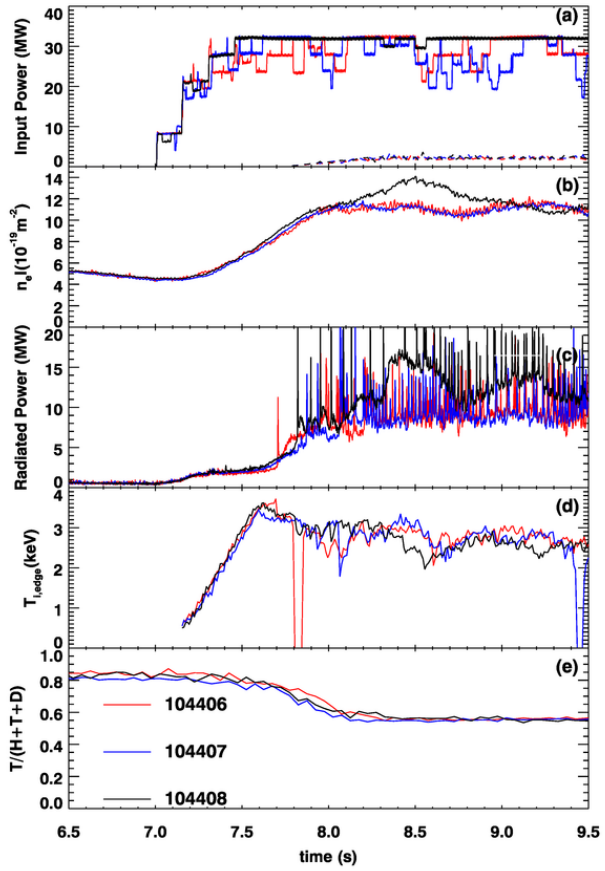

Figure 14: *Comparison of pulses at 3.85T with varying gas rates and performance. Input power, NBI solid and ICRH dashed (a), line integrated density (b), radiated power (c), edge ion temperature (d) and tritium concentration (e)*

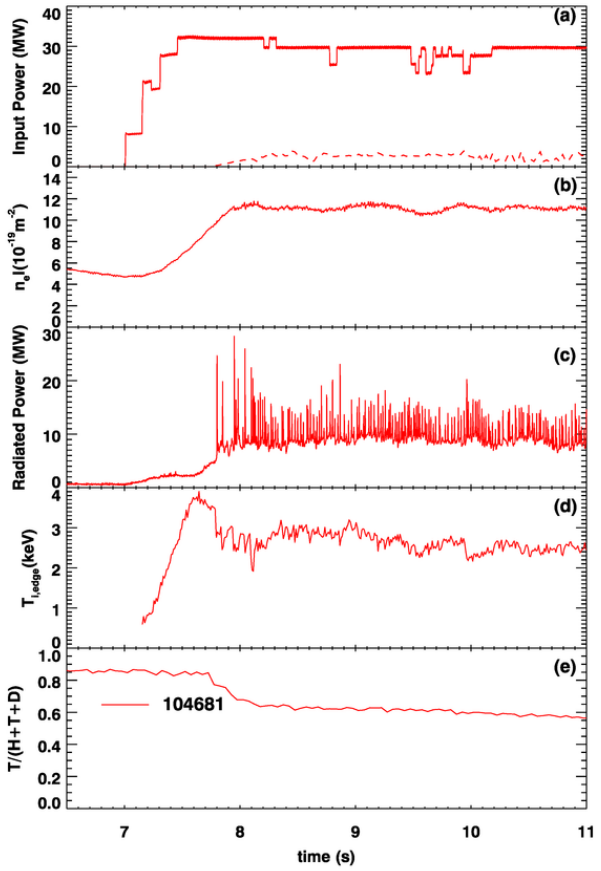

Figure 15: *Performance of DT plasma with no main chamber gas fuelling. Input power, NBI solid and ICRH dashed (a), line integrated density (b), radiated power (c), edge ion temperature (d) and tritium concentration (e)*

use of TIM15 from the density ramp as well as the main phase and instead use the same divertor TIM as used in the main phase. There was a reasonable probability this strategy would fail due to valve response being too slow for the required control of plasma density. The data from the previous dry runs was again used to estimate the required feed-forward waveform required for the density.

On the final day of the DTE3 campaign pulse 104681 without any fuelling from TIM15 was successful on the first attempt with a suitable density ramp to avoid temperature hollowness - data from the pulse is shown in Fig. 15. The pedestal performance of this pulse appeared to exceed that of the earlier pulses with the peripheral ion temperature ($\rho_{tor} \sim 0.85$) here exceeding 4keV in the overshoot phase and continuing at approximately 3keV for the main, ELMy phase of the pulse. This was in excess of any previous edge ion temperature observed on JET during the metallic wall period. Through the modification to the gas waveform for this pulse it appeared that the behaviour of the MHD was improved in this pulse, the β_N was slightly lower than a previous DT plasma (104408) and hence did not trigger a mode and allowing for more consistent performance, this is shown in Fig. 16

The goal of this experiment was not to maximise the fusion power produced, however for completeness the fusion power of the 3.45T and 3.85T plasmas are shown in Fig. 17. Despite the high NBI power (approaching maximum achievable on JET [23] [24]) fusion power could have been increased with adjustments to the isotope ratio and ICRH scheme if more experimental time had been available. In the initial phase of the plasma with the high ion temperature the fusion power would be increased if the isotope ratio was closer to 50:50 as the thermal fusion would be larger than the beam-target fusion at these temperatures if the isotope ratio was appropriate. Meanwhile, in the ELMy phase of the plasma where

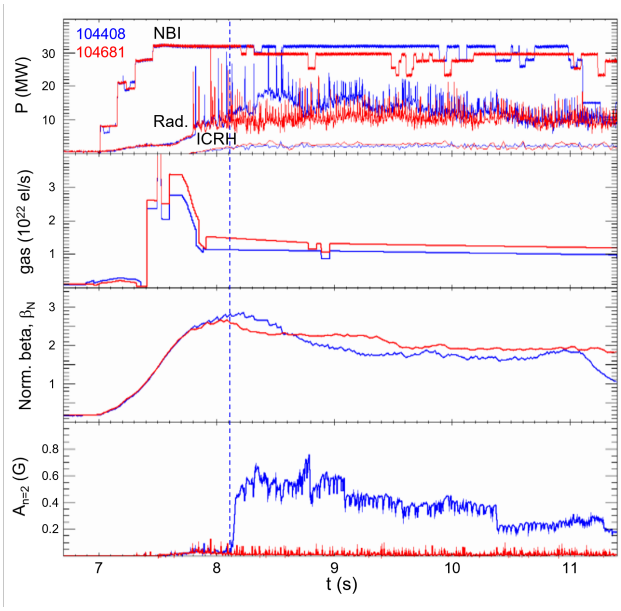

Figure 16: *Comparison of MHD behaviour between two DT plasmas. Input power, NBI solid and ICRH dashed (a), gas fuelling (b), normalised beta (c), and amplitude of n=2 mode (d)*

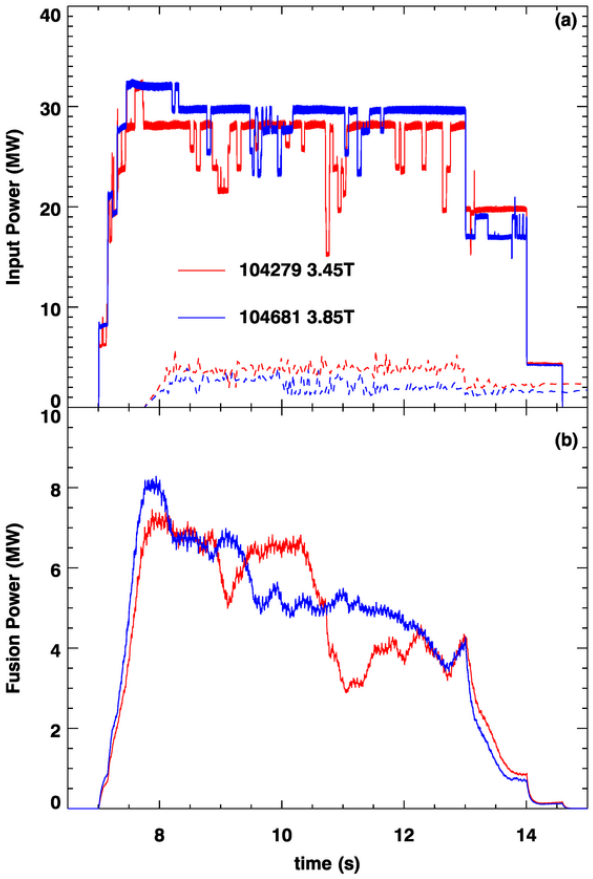

Figure 17: *Fusion power of pulses at 3.45T and 3.85T. NBI power (a) and fusion power (b).*

beam-target reactions dominate a more tritium rich plasma (as seen in the fusion power optimisation experiment [22] would generate a higher fusion power. Further to this, the ICRH scheme used in these plasmas generated core electron heating, a scheme that generated a synergy with the NBI power (again as in [22]) would have increased the fusion power, however those schemes are only of benefit with a tritium fraction of $\gtrsim 85\%$.

4.1. Deuterium Reference Plasmas

Following the DT campaign it was necessary to carry out some further deuterium reference pulses to ensure a good comparison was available, in particular for the 3.85T pulses that had not previously been carried out in D. Within these deuterium reference pulses some variation in the timing of the gas puff at the H-mode entry was carried out to ensure a good comparison was available. The plasmas were performed following the clean up of the tritium campaign. The two deuterium reference plasmas are compared with the DT pulse in Fig. 18. Within this phase of operations the pulses for the gas puff timing and pre-heat density described within section 2.1 were also performed. It can be seen that both deuterium pulses are similar to the DT pulse; the pulse with the earlier gas puff, 105508, has a matched density rise to the DT plasma but a slightly earlier first ELM due to the earlier gas while the pulse with the later gas puff, 105509, has a delayed increase to density and a similar timing of the first ELM to the DT pulse. The edge temperature and density in the main phase of each pulse is similar as shown in Fig. 19 providing a good basis for comparing how the main-ion isotope mass can change the impurity behaviour.

5. Screening Results

To determine if the plasmas are in the screening regime a time-dependent analysis of the bolometer data is performed as in [2]. This analysis shows if the transport of the tungsten is inwards or outwards at a given time, and in particular the difference between the ELM and inter-ELM transport. It is performed by examining the bolometer reconstruction and following the spatial and time dependence to determine if at a given location there is transport of the impurity inwards or outwards. There are assumptions made within this analysis, in particular that the total radiated power is dominated by tungsten and that the cooling factor of tungsten (as discussed in [2]) is approximately constant of the spatial range considered.

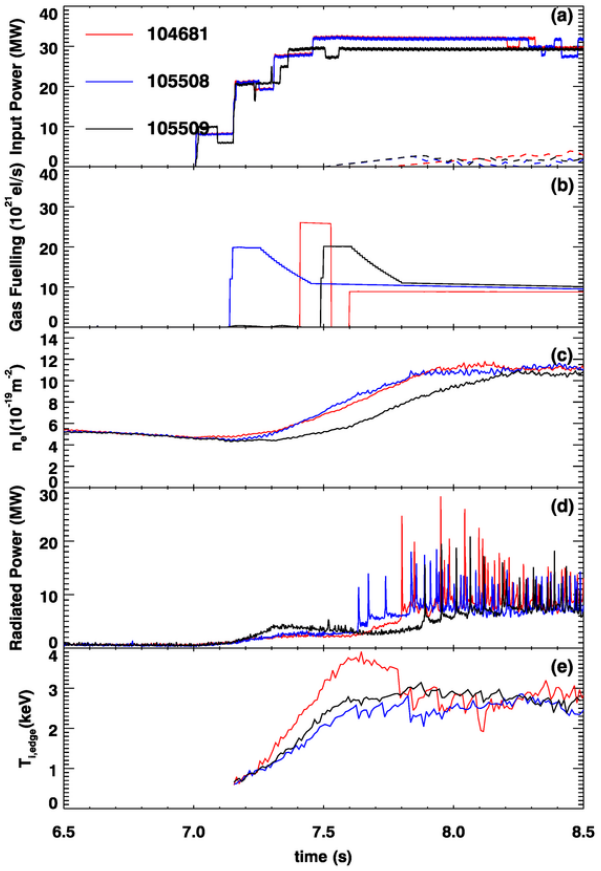

Figure 18: *Comparison of 3.85T D with DT plasmas. Shown in (a) is the heating power, NBI solid and ICRH dashed, (b) is the gas fuelling rate, (c) is the line integrated plasma density, (d) is the total radiated power and (e) is the edge ion temperature*

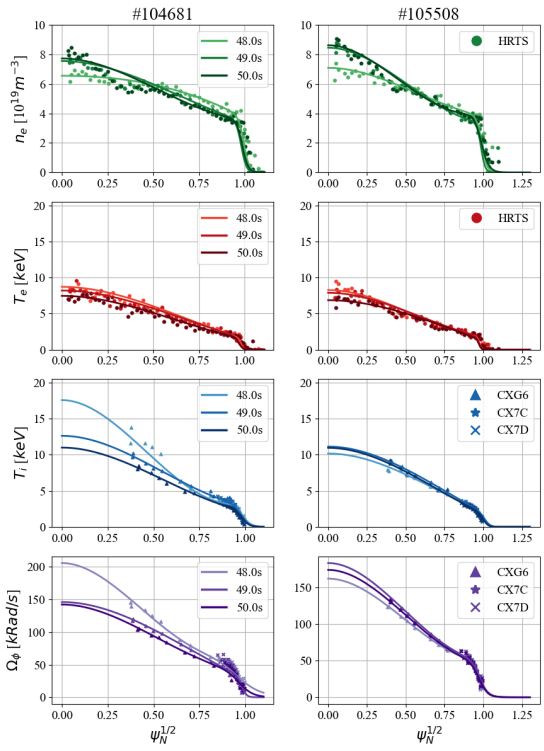

Figure 19: *Density (top), electron temperature (second), ion temperature (third) and rotation (bottom) for the DT (104681) and D (105508) plasmas at different times in the evolution of the pulse.*

These assumptions and the analysis method are more thoroughly described in [2]. It is expected that the peripheral density and temperature will affect the screening behaviour strongly, hence the average pedestal conditions over the heating phase in given plasmas are shown in Fig. 20.

The screening vs flushing analysis for a series of pulses is shown in the following figures. Within these figures multiple time points within the main heating phase of the pulse are shown with the transport of impurities during an ELM shown on the y-axis and inter-ELM transport shown on the x-axis, negative transport referring to outward, removal of impurities. Points within the upper left quadrant show inter-ELM screening while points in the lower right quadrant demonstrate ELM flushing. Fig. 21 shows how the variation in plasma current as in pulses 102813 (2.3MA) and 102825 (2.3MA) can affect the screening. While both pulses demonstrate screening the pulse at

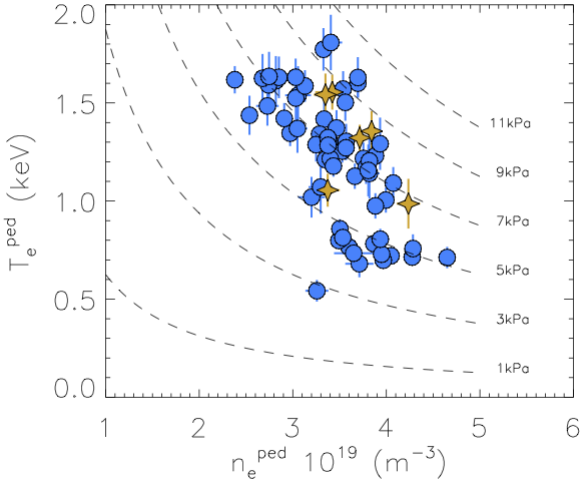

Figure 20: *Average T_e^{ped} vs N_e^{ped} during main phase of pulses (following the performance overshoot). Blue points are D plasmas while gold points are D-T plasmas*

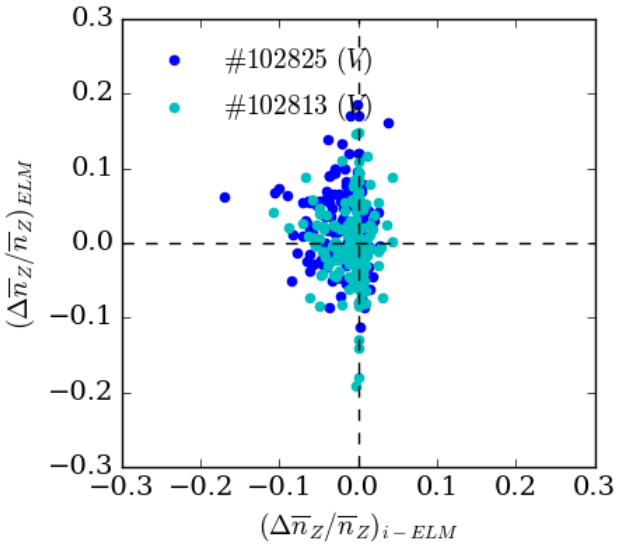

Figure 21: *A comparison of the relative changes in the W content of the plasma due to ELM flushing $(\triangle\bar{n}_W/\bar{n}_W)_{ELM}$ vs the change due to the inter-ELM influx $(\triangle\bar{n}_W/\bar{n}_W)_{i-ELM}$ for plasmas at 2.1MA (green, 102813) and 2.3MA (blue, 102825).*

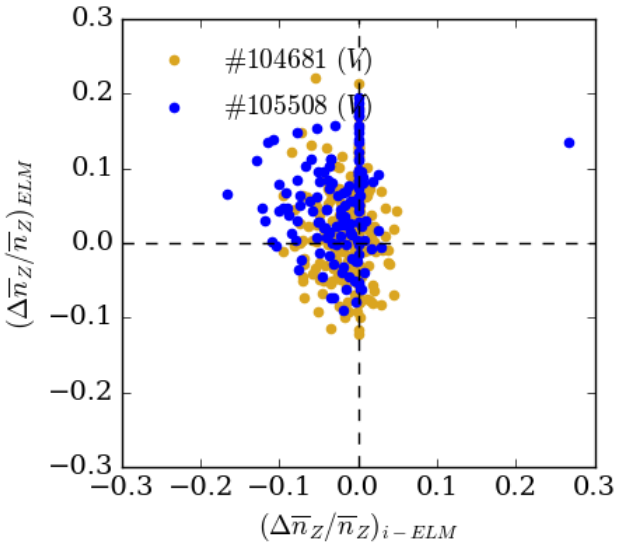

Figure 22: *A comparison of the relative changes in the W content of the plasma due to ELM flushing $(\triangle\bar{n}_W/\bar{n}_W)_{ELM}$ vs the change due to the inter-ELM influx $(\triangle\bar{n}_W/\bar{n}_W)_{i-ELM}$ for plasmas deuterium (blue, 105508) and DT (gold, 104681).*

lower plasma current appears to have more timepoints in the upper left and deeper into that quadrant although this difference is marginal. The comparison of the D and D-T plasmas are shown in Fig. 22, both pulses demonstrate many time points in the screening regime with no major difference seen in this figure even though the D plasma has lower impurity radiation in total compared to the D-T plasma. These pulses show screening more clearly than the previous example, 97781 and the DTE2 results. Finally, the comparison of the pulses with different gas puff timing is shown, both have many time points in the screening regime again while the earlier gas puff appears to have marginally more time points in the flushing regime than the later gas puff. Further analysis of these data including interpretation with respect to neo-classical expectations are published separately in [9].

6. Conclusions

A series of hybrid plasmas have been developed to further test the peripheral impurity screening previously demonstrated on JET. Successful, inter-ELM screening of the impurities has been observed through analysis of the bolometer data in a range of plasma conditions. In particular, a range of pedestal densities and temperatures have been explored. The development of DT plasmas with gas fuelling optimised for diagnostic coverage has allowed the confirmation of screening results in DT operation on JET. The operational and scenario development steps required to

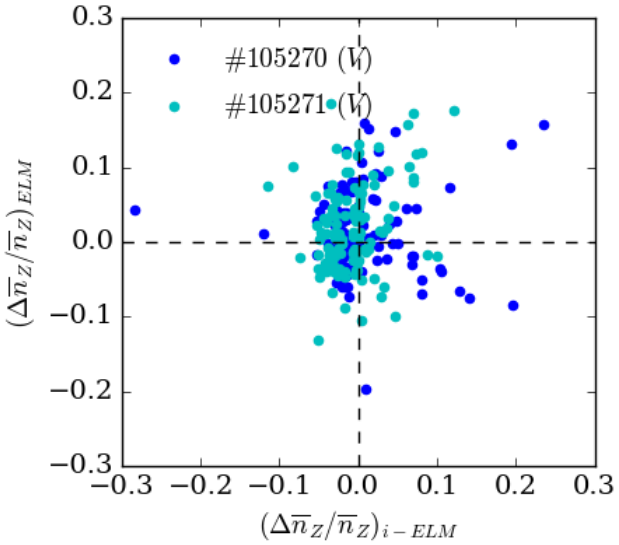

Figure 23: *A comparison of the relative changes in the W content of the plasma due to ELM flushing $(\triangle\bar{n}_W/\bar{n}_W)_{ELM}$ vs the change due to the inter-ELM influx $(\triangle\bar{n}_W/\bar{n}_W)_{i-ELM}$ for plasmas with earlier gas puff (blue, 105270) and later gas puff (green, 105271).*

obtain the results have been discussed, with a focus on how precise timing and setup of gas fuelling is essential to an optimised scenario. The methods discussed provide information on some of the tools required for the development of a plasma scenario from deuterium to deuterium-tritium operation. While this experience requires adjustment to specific operating conditions and plasma scenario it will still provide guidance for the efficient operation of upcoming fusion experiments

The analysis of the data combined with the calculations of possible neo-classical screening are the subject of a further work [9]. The isotope dependence of the screening effect is a complex combination of different effects but the increased ion temperature of the DT plasmas is promising for the consideration of ITER and other reactor concepts beyond this.

This work has been carried out within the framework of the EUROfusion Consortium, funded by the European Union via the Euratom Research and Training Programme (Grant Agreement No 101052200 EUROfusion) and from the EPSRC [grant number EP/W006839/1]. To obtain further information on the data and models underlying this paper please contact PublicationsManager@ukaea.uk. Views and opinions expressed are however those of the author(s) only and do not necessarily reflect those of the European Union or the European Commission. Neither the European Union nor the European Commission can be held responsible for them.

7. References

[1] Angioni C et al. 2018 *Physics of Plasmas* **25** 082517
[2] Field A et al. 2022 *Nucl. Fusion* **63**, 016028
[3] Challis C D et al. 2015 *Nucl. Fusion* **55** 053031
[4] Hobirk J et al. *Nucl. Fusion* **63**, 112001
[5] Maggi C F et al 2024 *Nucl. Fusion* **64**, 112021
[6] Kappatou A et al. 2025 *Plasma Phys. and Contr. Fusion* **67**, 045039
[7] The JET Operations Team (presented by D.B. King) et al 2024 *Nucl. Fusion* **64**, 106014
[8] Fajardo D et al. 2023 *Plasma Phys. and Contr. Fusion* **65**, 035021
[9] Field, A R et al submitted
[10] Garcia J. et al. 2023 *Nucl. Fusion* **63** 112003
[11] Negus C R et al 2006 *Rev. Sci. Inst* **77** 10F102
[12] Andrew Y and Hawkes N C 2006 *Rev. Sci. Inst* **77** 10E913
[13] Kirov K.K. et al. 2019 *Nucl. Fusion* **59** 056005
[14] Duesing G et al. 1987 (*Fus Sci. Technology*) Vol. **11** 163-202
[15] Felton R et al 2025 *Plasma Phys. and Contr. Fusion* **67**, 095020
[16] I Monakhov et al 2025 *Plasma Phys. and Contr. Fusion* **67**, 015023
[17] Challis C D et al. 2020 *Nucl. Fusion* **60** 086008
[18] Solano E R et al. 2023 *Nucl. Fusion* **63** 112011
[19] Schneider P A et al 2023 *Nucl. Fusion* **63** 112010
[20] Frassinetti L et al 2023 *Nucl. Fusion* **63** 112009
[21] Martin Y R et al. 2008 *J. Phys.: Conf. Ser.* **123** 012033
[22] Maslov M et al. 2023 *Nucl. Fusion* **63** 112002
[23] King D B et al accepted
[24] King D B et al 2023 *Nucl. Fusion* **63** 112005